Am J Transl Res 2021;13(10):11048-11064
www.ajtr.org /ISSN:1943-8141/AJTR0131863

Original Article

TNFSF13B and *PPARGC1A* expression is associated with tumor-infiltrating immune cell abundance and prognosis in clear cell renal cell carcinoma

Tianming Ma[1,2], Lingfeng Meng[1,2], Xiaonan Wang[2,3], Zijian Tian[1,2], Jiawen Wang[1], Xiaodong Liu[1,2], Wei Zhang[1], Yaoguang Zhang[1,2]

[1]Department of Urology, Beijing Hospital, National Center of Gerontology, Institute of Geriatric Medicine, Chinese Academy of Medical Sciences, Beijing 100730, China; [2]Graduate School of Peking Union Medical College, Chinese Academy of Medical Sciences, Beijing 100730, China; [3]Department of Radiology, Beijing Hospital, National Center of Gerontology, Institute of Geriatric Medicine, Chinese Academy of Medical Sciences, Beijing 100730, China

Received February 14, 2021; Accepted August 7, 2021; Epub October 15, 2021; Published October 30, 2021

Abstract: Growing evidence suggests that the tumor microenvironment (TME) plays crucial roles in tumor progression and treatment efficacy in clear cell renal cell carcinoma (ccRCC), which typically has a poor prognosis due to high relapse and metastasis rates. We comprehensively analyzed ccRCC RNA-sequencing data from The Cancer Genome Atlas (TCGA) database to identify candidate prognostic TME-related genes involved in ccRCC. We used the ESTIMATE and CIBERSORT algorithms to estimate the proportions of immune cells, stromal cells, and tumor-infiltrating immune cells (TICs) in the TME in ccRCC samples from 539 patients. By examining the intersection of the differentially expressed genes (DEGs) obtained by Cox regression analysis and protein-protein interaction network, we identified five overlapping DEGs (*IGLL5*, *MZB1*, *HSD11B1*, *TNFSF13B*, and *PPARGC1A*). Further analysis revealed that *TNFSF13B* expression was elevated in ccRCC tumor tissues and negatively associated with overall survival. *PPARGC1A* expression exhibited the opposite patterns. Immunohistochemical analysis of 35 paired ccRCC and adjacent normal tissues confirmed the in-silico results. Gene set enrichment analysis revealed that genes in the groups with high *TNFSF13B* and *PPARGC1A* expression were enriched mainly in immune-related activities. In the group with low *PPARGC1A* expression, genes were enriched in metabolic pathways. CIBERSORT analysis of TIC proportions revealed that Tregs and CD8 T-cell abundance correlated positively with *TNFSF13B* expression, but negatively with *PPARGC1A* expression. These findings demonstrate that *TNFSF13B* and *PPARGC1A* are prognostic predictors and possible therapeutic targets in ccRCC.

Keywords: *TNFSF13B*, *PPARGC1A*, tumor microenvironment, tumor-infiltrating immune cell, clear cell renal cell carcinoma

Introduction

Kidney cancer is a common type of cancer with a high mortality rate and a steadily increasing morbidity rate worldwide [1]. In 2020, there were ca. 73,750 new cases of kidney cancer and ca. 14,830 deaths due to kidney cancer in the USA [2]. Renal cell carcinoma (RCC) is the major histological type, accounting for approximately 90% of all kidney cancers. Clear cell renal cell cancer (ccRCC) is the most common subtype. Although surgery is effective for early stage ccRCC, early diagnosis is difficult. Relapse or metastasis occur in 30% of cases after curative treatment. Unfortunately, the prognosis of patients with metastasis is generally poor because ccRCC is insensitive to conventional radiotherapy and chemotherapy [3]. It is imperative to elucidate the mechanisms underlying the development of ccRCC.

Recent studies have reported the significance of the tumor microenvironment (TME) in cancer development and progression [4, 5]. Resident stromal cells and recruited immune cells play important roles in the TME and contribute to tumor progression. The precise mechanisms remain unclear [6]. The roles of tumor-infiltrat-

ing immune cells (TICs) in the TME in tumorigenesis and immunotherapy have been studied [7, 8]. TIC abundance is known to be significantly correlated with outcomes in ccRCC [9, 10].

The ESTIMATE and CIBERSORT algorithms have been widely used to estimate the contributions of immune and stromal cells to TICs in the TMEs of various cancers, including ccRCC [11-13]. We used these tools to examine the proportions of TICs, immune cells, and stromal cells in ccRCC tissues. We investigated the expression of TME-related genes and their associations with clinical prognosis and TICs using data from The Cancer Genome Atlas (TCGA) database and our hospital.

Materials and methods

Data sources

We collected transcriptome RNA-sequencing data from tumor tissues and corresponding clinical data from 539 ccRCC patients, along with data from 72 adjacent non-tumor samples, from TCGA. The ESTIMATE algorithm was used to calculate immune, stromal, and ESTIMATE scores for each sample. These scores represent the ratios of immune-stromal components and their total proportions in the TME. Xie et al. collected gene expression profiling data and clinical follow-up information from 629 ccRCC cases from the Gene Expression Omnibus database (datasets GSE29609, GSE22541, and GSE3) and TCGA to develop the web tool OSkirc (http://bioinfo.henu.edu.cn/KIRC/KIRCList.jsp), which we used to validate our results [14]. Further, 35 patients with ccRCC who underwent surgical treatment in Beijing Hospital between January 2013 and December 2020 were enrolled in this study for immunohistochemical analysis of their tissue samples. This research was approved by the Research Ethics Committee of Beijing Hospital (approval number: 2021BJYYEC-161-01). Informed consent was acquired from all patients involved.

Analysis of the associations between ESTIMATE scores, overall survival (OS), and clinicopathology

The tumor samples from TCGA were divided into high- and low-immune-, stromal-, and ESTIMATE-score groups based on the median scores. Kaplan-Meier curves were generated to compare OS of ccRCC patients between the groups. The Wilcoxon rank-sum test or Kruskal-Wallis rank sum test was used to evaluate the relationship between the scores and clinicopathological parameters.

Differentially expressed genes (DEGs) identification

We used the Wilcoxon rank-sum test to identify DEGs between the high- and low-score groups based on a |log foldchange| >1 and a false discovery rate (FDR) <0.05. Heatmaps of the DEGs were created using the R package pheatmap.

DEGs enrichment analysis

The functions of the DEGs identified were elucidated using Gene Ontology (GO) and Kyoto Encyclopedia of Genes and Genomes (KEGG) enrichment analyses using the R packages clusterProfiler, enrichplot, and ggplot2. Terms with $P<0.05$ and $q<0.05$ were considered significantly enriched.

Protein-protein interaction (PPI) network and Cox regression analyses

A PPI network of the DEGs was established using the STRING database, set to 0.4, and was reconstructed using Cytoscape v. 3.6.1. Univariate Cox regression analysis was used to identify prognostic genes among the DEGs. We integrated the results of these two analyses to determine hub genes.

Analysis of the associations between hub gene expression, OS, and clinicopathology

The R package limma was used to visualize the differential expression of the hub genes in the normal and ccRCC tissue samples from TCGA. The samples were classified into low- or high-expression groups for each hub gene based on the median expression. Survival analysis was used to compare OS between the two groups. The Wilcoxon rank-sum test was used to determine the relationship between hub gene expression and clinicopathological parameters.

Gene set enrichment analysis (GSEA) of the hub genes

We conducted GSEA with the C2 KEGG v. 7.1 and C7 v. 6.2 gene sets using GSEA v. 4.0.3. A nominal P and FDR $q<0.05$ indicated significance.

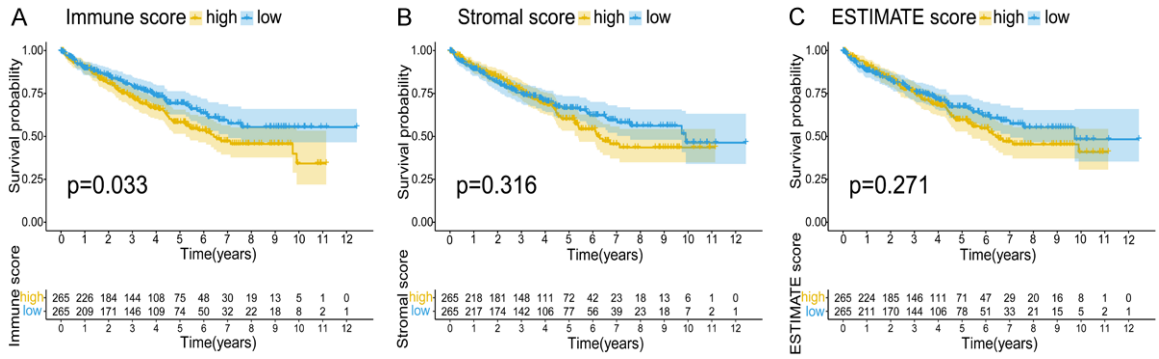

Figure 1. Correlation between ESTIMATE scores and the OS of ccRCC patients. Kaplan-Meier survival analysis of ccRCC patients grouped by (A) immune score, (B) stromal score, and (C) ESTIMATE score.

Analysis of the correlations between hub gene expression and the proportion of TICs

We used the CIBERSORT algorithm (downloaded from https://cibersortx.stanford.edu/) to estimate the proportion of TICs. Only those tumor samples with $P<0.05$ in terms of quality filtering were retained to evaluate the correlations between TICs and hub genes.

Statistical analysis

All analyses were performed using R v.4.0.3 (http://www.R-project.org). The Wilcoxon rank-sum test was used to compare gene expression between tumor and normal tissues and subgroups based on clinicopathological parameters. The Kruskal-Wallis test was used for comparisons of more than two groups. Kaplan-Meier analysis and the log rank test were used to assess OS in the different groups. Univariate Cox regression analysis was used to screen out prognostic genes among the DEGs. The Wilcoxon rank-sum test was used to compare the difference of TICs between high- and low-expression groups of hub genes. Spearman correlation analysis was used to investigate the correlations between TICs and hub genes. Statistical significance was set at $P<0.05$.

Results

The ESTIMATE immune score is negatively correlated with OS

Tumor samples were classified into high- and low-score groups based on the median ESTIMATE scores. According to Kaplan-Meier curves, patients with a high immune score had a more damaged OS than those with a low immune score ($P=0.033$, **Figure 1A**). OS did not significantly differ between the low- and high-score groups for the stromal or ESTIMATE scores (**Figure 1B**, **1C**). This indicates that the immune component of the TME is a better indicator of ccRCC prognosis than the stromal component.

The ESTIMATE immune score correlates with clinicopathology

ccRCC patients aged ≤65 years had higher stromal scores than older ccRCC patients ($P=0.0064$, Wilcoxon rank-sum test) (**Figure 2G**). The immune and ESTIMATE scores did not significantly differ between older and younger patients (**Figure 2A**, **2M**). The immune and ESTIMATE scores increased with pathologic grade (G1 vs. G4, G2 vs. G3, G2 vs. G4, G3 vs. G4, all $P<0.05$; **Figure 2B**, **2N**). Similar results were obtained for clinical stage (stage I vs. stage III, stage I vs. stage IV, $P<0.05$; **Figure 2C**, **2O**). The immune and ESTIMATE scores were both higher in T3 than in T1 ($P<0.05$; **Figure 2D**, **2P**) and in M1 than in M0 ($P<0.05$; **Figure 2F**, **2R**). None of the three scores were significantly correlated with N stage (**Figure 2E**, **2K**, **2Q**). These findings provide evidence that the immune and stromal components affect the progress of ccRCC.

Detection and enrichment of DEGs

The Wilcoxon rank-sum test was used to assess the significance of differential gene expression between the immune and stromal score groups. Notably, 656 DEGs were obtained from immune score (samples with high score vs. low

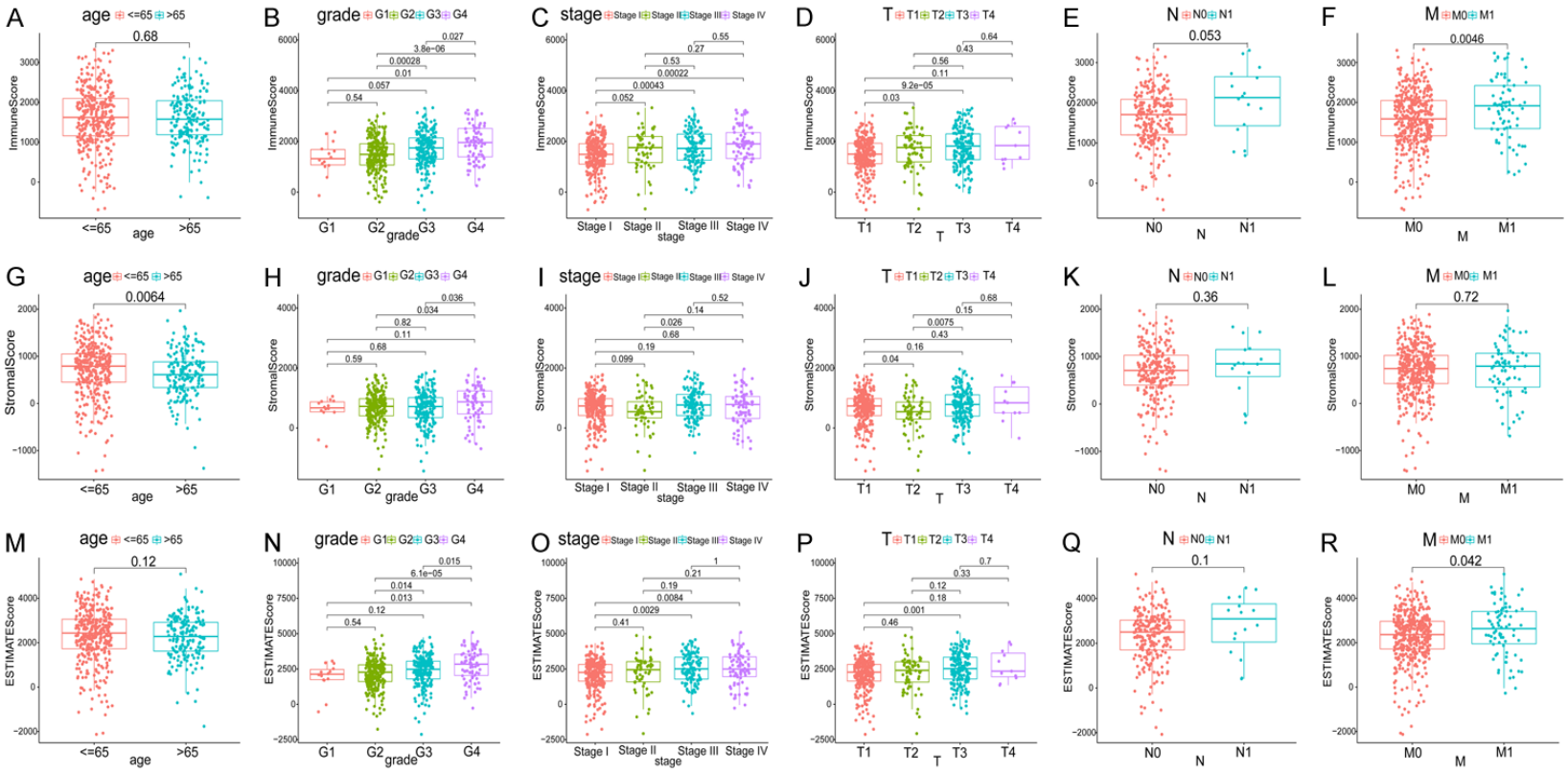

Figure 2. Relationship between scores and clinicopathological characteristics of ccRCC patients. (A-F) Immune scores according to age, pathological grade, clinical stage, and TNM stage. (G-L) Stromal and (M-R) ESTIMATE scores according to clinicopathology.

score). Among them, 510 genes were upregulated, and 146 genes were downregulated (**Figure 3A**, **3C**, **3D**). There were 411 DEGs in the high-stromal-score vs. low-stromal-score group (259 upregulated and 152 downregulated, respectively) (**Figure 3B-D**). A Venn diagram revealed 93 overlapping DEGs between the stromal and immune groups (44 upregulated and 49 downregulated), which may play important roles in the TME. GO and KEGG enrichment analyses were used to elucidate the roles of these 93 DEGs. Most were associated with immune-related activities, including leukocyte proliferation and cytokine-cytokine receptor interactions (**Figure 3E**, **3F**).

PPI network and prognostic genes

To elucidate the relationship among the DEGs, we established a PPI network, which comprised 52 DEGs and 93 edges (**Figure 4A**). **Figure 4B** shows the top 30 hub genes, ranked according to their connectedness in the PPI network (i.e., the number of nodes they connect to). Cox regression analysis identified 23 prognostic DEGs among the 93 overlapping DEGs (**Figure 4C**). By integrating the results of these two analyses, we found five genes related to prognosis: *IGLL5*, *MZB1*, *HSD11B1*, *TNFSF13B*, and *PPARGC1A* (**Figure 4D**).

TNFSF13B and PPARGC1A expression correlates with prognosis

The expression of the five hub genes differed significantly between normal and ccRCC tissues. The ccRCC samples were classified into high- and low-expression groups based on the median expression of the five hub genes. Among these genes, *TNFSF13B* and *PPARGC1A* showed the largest expression differences between the normal and ccRCC samples and the strongest association with OS. Elevated *PPARGC1A* expression was associated with improved OS in ccRCC patients (**Figure 5**). These two genes were selected for further comprehensive analysis.

TNFSF13B and PPARGC1A protein expression in ccRCC was evaluated by immunohistochemistry using 35 paired ccRCC and adjacent normal tissues from patients treated in our center. The protein expression data were consistent with the mRNA expression data from TCGA (i.e., high *TNFSF13B* expression in ccRCC tissues, but low *TNFSF13B* expression in adjacent normal tissues, and high *PPARGC1A* expression in adjacent normal tissues, but low *PPARGC1A* expression in ccRCC tissues) (**Figure 6**). The Kaplan-Meier analysis in OSkirc showed that elevated *TNFSF13B* expression was closely related to worsened OS in ccRCC patients ($P<0.001$, **Figure 7A**). Elevated *PPARGC1A* expression was associated with improved OS in ccRCC patients ($P<0.001$, **Figure 7B**). These findings were consistent with our results.

Correlations between hub gene expression and clinicopathological parameters of ccRCC patients

We found that *TNFSF13B* expression increased with increasing grade, clinical stage, and TNM stage (**Figure 8A-E**). *PPARGC1A* expression decreased with increasing grade, clinical stage, and T and M stages, but not N stage (**Figure 8F-J**). These findings suggest that *TNFSF13B* and *PPARGC1A* may influence disease progression and patient survival in ccRCC.

TNFSF13B and PPARGC1A functional enrichment analyses

To determine the functions of *TNFSF13B* and *PPARGC1A* in ccRCC, GSEA was applied to the high- and low-expression groups compared with the median level of these two genes expression, respectively. Samples with high expression of these two genes were enriched in genes related to cell adhesion- and immune-related activities, including extracellular matrix-receptor interaction, focal adhesion, and B-cell and T-cell receptor signaling pathways, among the C2 KEGG and C7 immune gene sets (**Figure 9A**, **9C**, **9D**, **9F**). Samples with low *PPARGC1A* expression were enriched in genes involved in metabolic pathways, including PPAR signaling and leucine and isoleucine degradation (**Figure 9E**). For C7 immune gene sets, based on the criterion FDR $q<0.5$, there were no gene sets enriched in the low expression group of two hub genes.

TNFSF13B and PPARGC1A expression regulates TME immune activity

We used the CIBERSORT algorithm to estimate the number of TIC subsets among the ccRCC samples. There were 22 distinct TIC profiles (**Figure 10**). By combining difference and cor-

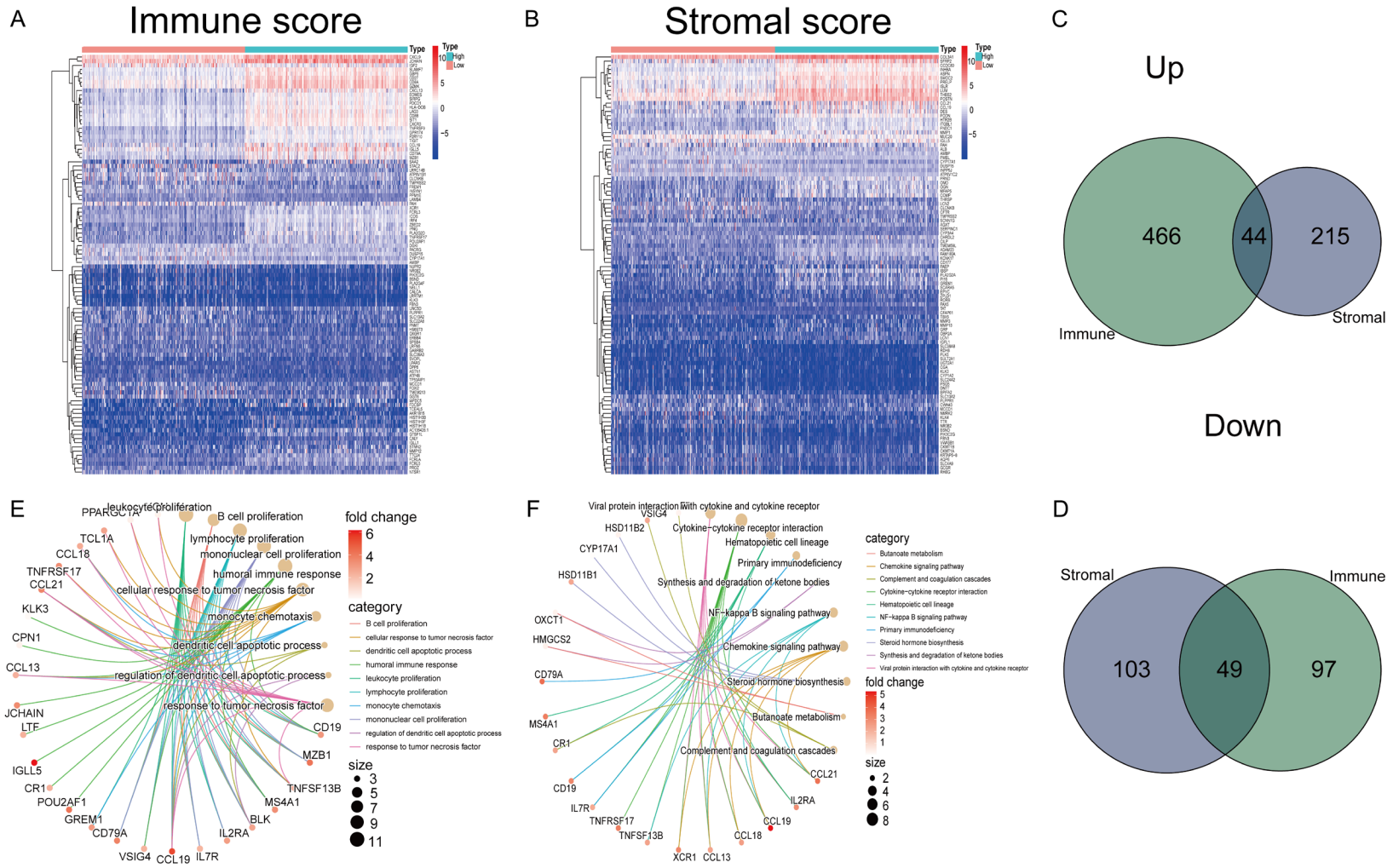

Figure 3. Analysis of DEGs. Heatmaps for DEGs generated by comparison of the high score group vs. the low score group in (A) immune and (B) stromal scores. (C, D) Venn diagrams showing common upregulated and downregulated DEGs associated with immune and stromal scores. (E, F) GO and KEGG enrichment analysis of 93 DEGs.

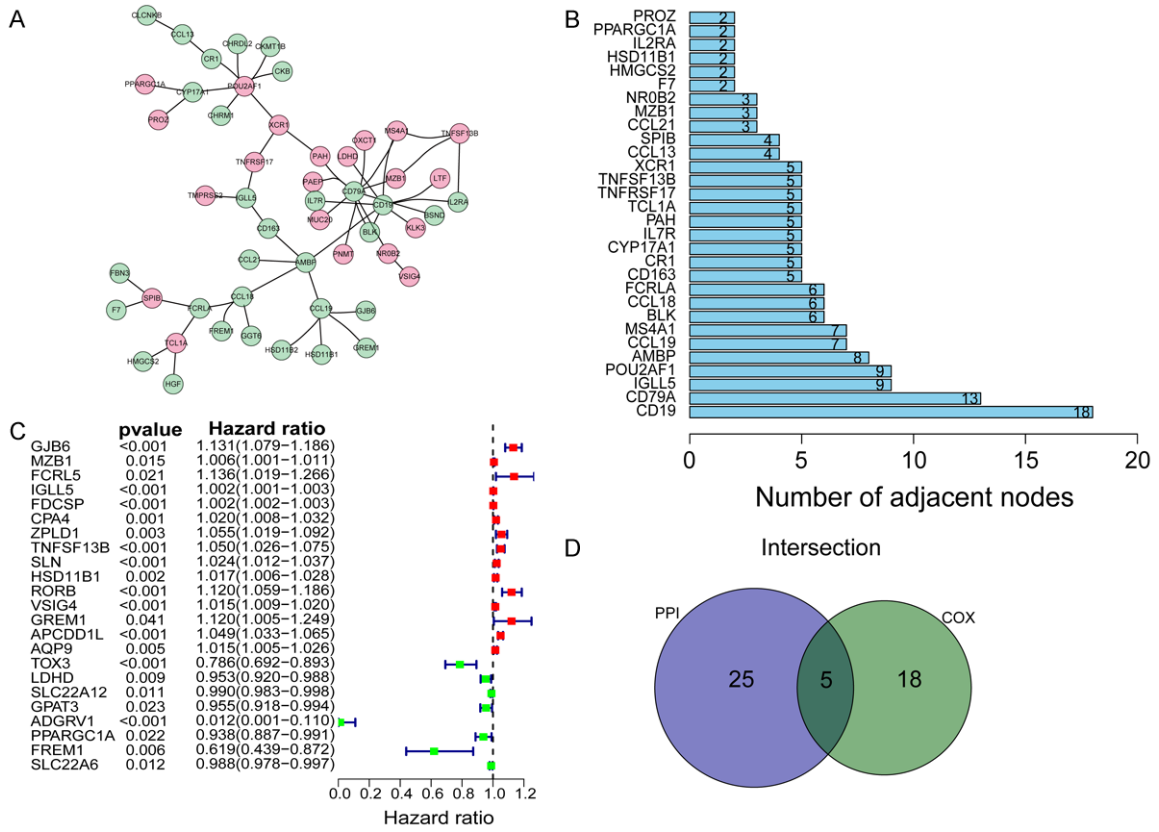

Figure 4. PPI network and determination of hub genes. A. PPI network, the confidence threshold was set to 0.4. B. Bargraph showing the top 30 hub genes, ranked according to their connectedness in the PPI network (i.e., the number of nodes they are connected with). C. Forest plot of the 23 prognostic genes generated by univariate Cox analysis with P<0.05. D. Venn diagram showing the common hub genes shared by leading 30 nodes in PPI and significant factors in univariate Cox.

relation analyses, we found that 11 types of TICs were correlated with *TNFSF13B* expression: naive B cells, activated dendritic cells, eosinophils, resting mast cells, resting NK cells, activated memory CD4 T cells, resting memory CD4 T cells, CD8 T cells, follicular helper T cells, gamma delta T cells, and regulatory T cells (Tregs) (**Figure 11B-E**, **11H**, **11J-P**); most of the associations were positive. Similarly, 10 types of TICs were correlated with *PPARGC1A* expression (**Figure 12C**, **12E-I**, **12K-O**). Of these, Tregs showed the most significant correlation. These findings suggested that both *TNFSF13B* and *PPARGC1A* have immunomodulatory roles in the TME.

Discussion

RCC tumors are complex and heterogeneous tumors with high recurrence and metastasis rates. The prognosis of RCC patients is usually dismal [15]. For a number of years, tyrosine kinase inhibitors, which inhibit the vascular endothelial growth factor receptor, have been used to treat metastatic RCC [16]. Unfortunately, because of drug resistance, only a small proportion of patients benefit from tyrosine kinase inhibitors [17]. TICs have been suggested to impact resistance to tyrosine kinase inhibitors in the TME [10, 18].

There is increasing evidence of the clinical significance of the TME in predicting tumorigenesis, progression, prognosis, and therapeutic efficacy, in which TICs in the TME play important roles [4-10]. Recently, immune checkpoint inhibitors have been recommended as a first-line treatment for metastatic RCC [19, 20]. The TME is actively involved in the response to immune checkpoint inhibitors [21]. By conducting a comprehensive ccRCC RNA-sequencing data analysis using TCGA data, we identified five TME-related genes (*IGLL5*, *MZB1*, *HSD11B1*, *TNFSF13B*, and *PPARGC1A*) that

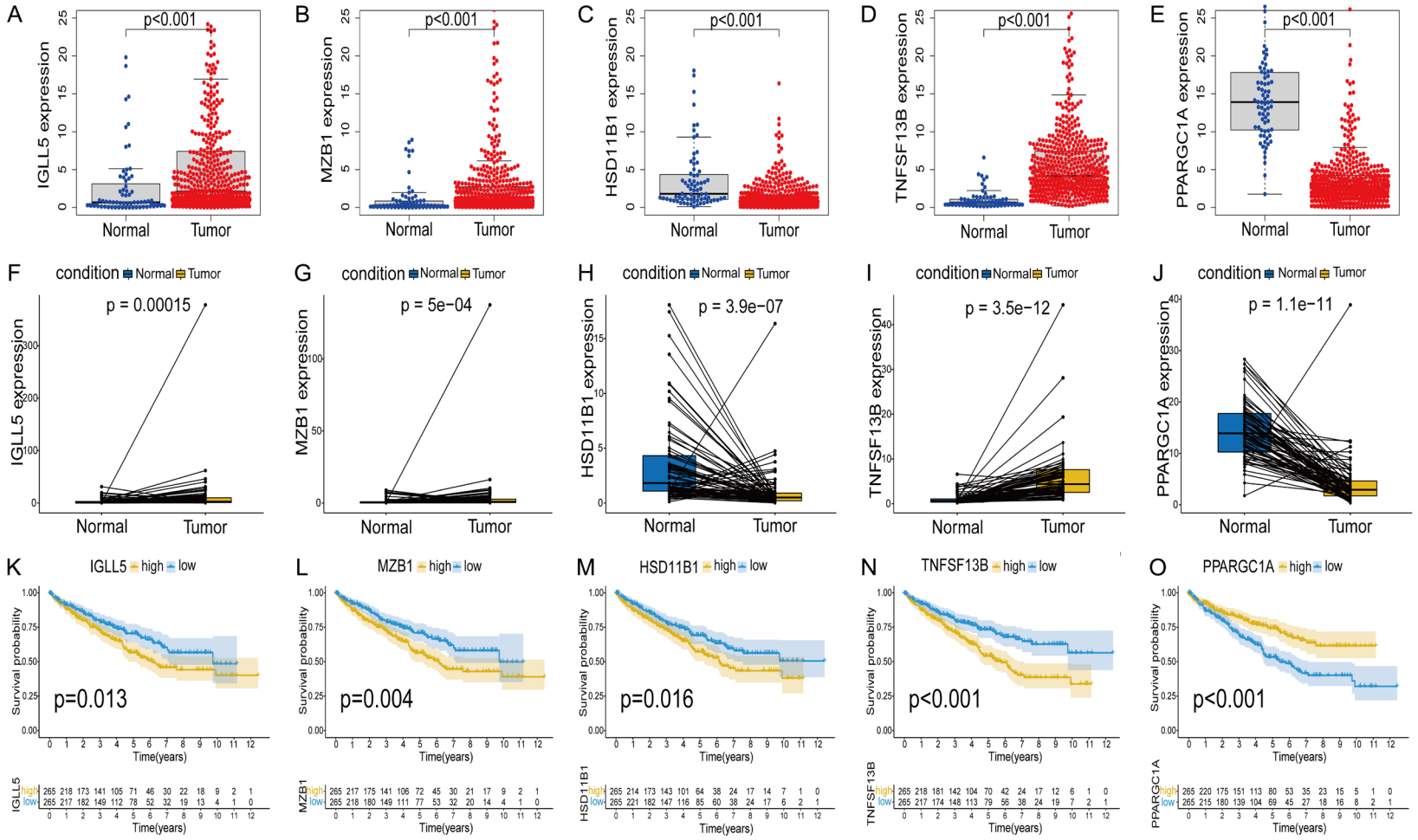

Figure 5. Expression of TME-related candidate prognostic genes in ccRCC tissues and associations between gene expression and OS in ccRCC patients. A-E. Differential expression of IGLL5, MZB1, HSD11B1, TNFSF13B, and PPARGC1A between normal and tumor samples. F-J. Paired differentiation analysis of hub genes. K-O. OS of ccRCC patients according to high or low hub gene expression.

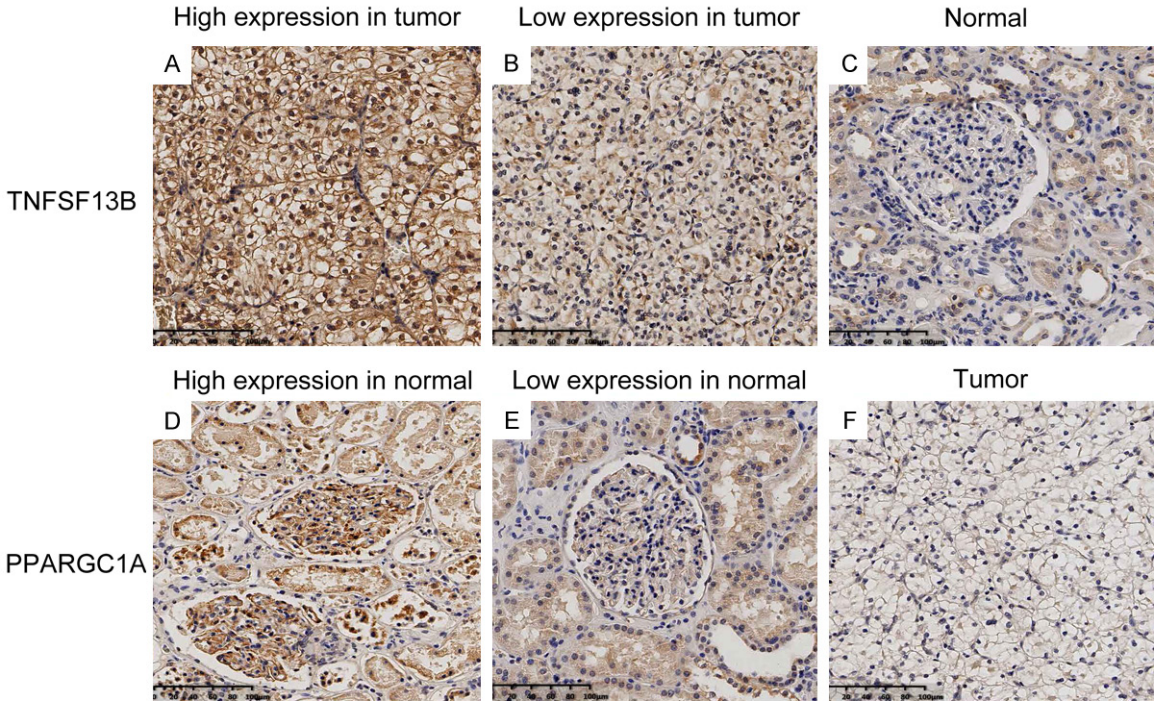

Figure 6. Immunohistochemical staining of TNFSF13B and PPARGC1A in ccRCC tumor and adjacent normal tissues. A. High TNFSF13B expression in ccRCC tissues; B. Low TNFSF13B expression in ccRCC tissues; C. Low TNFSF13B expression in adjacent normal tissues; D. High PPARGC1A expression in adjacent normal tissues; E. Low PPARGC1A expression in adjacent normal tissues; F. Low PPARGC1A expression in ccRCC tissues. Scale bar: 100 μm. Magnification: 200×.

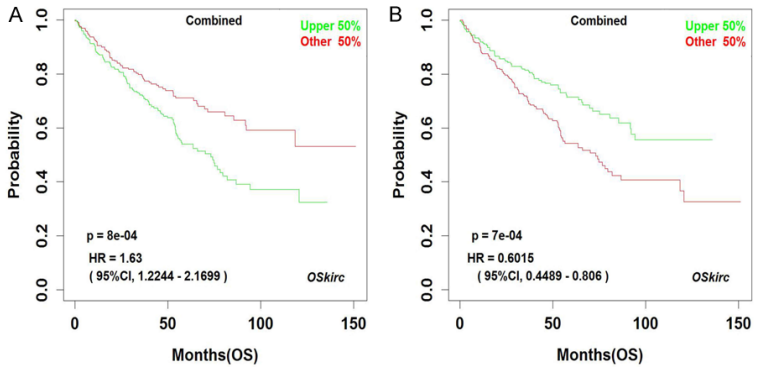

Figure 7. Kaplan-Meier analysis of patients with high and low expression of TNFSF13B (A) and PPARGC1A (B) in the OSkirc web tool.

may have prognostic value in ccRCC. We elucidated the prognostic significance of *TNFSF13B* and *PPARGC1A* expression and screened immune cells associated with the expression of these two genes. The findings suggested *TNFSF13B* and *PPARGC1A* be prognostic markers and novel therapeutic targets in ccRCC.

TNFSF13B, also known as *BAFF*, encodes tumor necrosis factor ligand superfamily member 13B, which regulates B-cell differentiation and survival, and T-cell function [22, 23]. Extensive evidence suggesteds it plays a prominent role in immune system diseases [24, 25]. Its function in glioma and breast tumors has been examined [26, 27]. In ccRCC, *TNFSF13B* expression is positively correlated with tumor stage [28]. Consistent with findings in previous studies [12, 28], the current study revealed that elevated *TNFSF13B* expression in ccRCC was significantly positively associated with histological grade, clinical stage, TNM stage, and with poor prognosis. We attempted to further elucidate its role in ccRCC using GSEA, which revealed that *TNFSF13B* upregulation was associated with immune-related signaling pathways, such as the B-cell and macrophage receptor signaling pathways. Stelmach et al. identified seven alternative *TNFSF13B* transcripts in T-cell and monocyte transcriptomes and found that

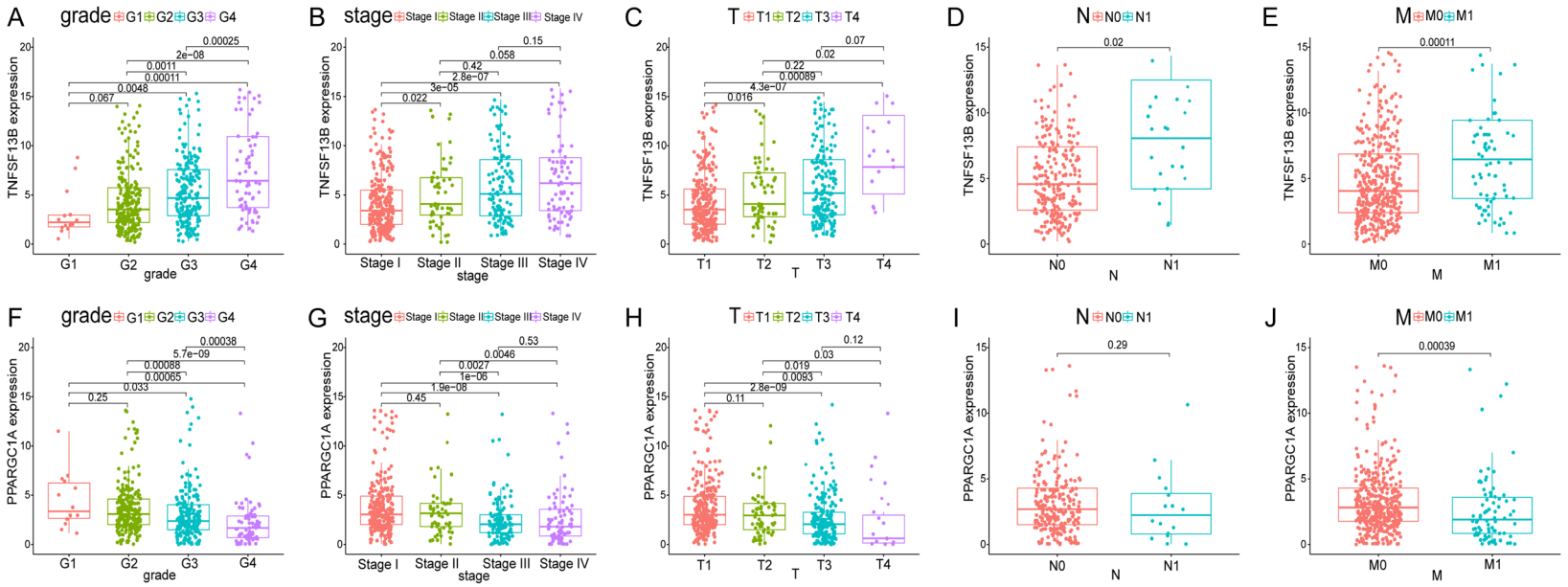

Figure 8. Clinicopathologic significance of TNFSF13B and PPARGC1A expression in ccRCC tissues. Influence of TNFSF13B expression on (A) pathological grade, (B) clinical stage, and (C-E) TNM stages. Influence of PPARGC1A expression on (F) pathological grade, (G) clinical stage, and (H-J) TNM stages.

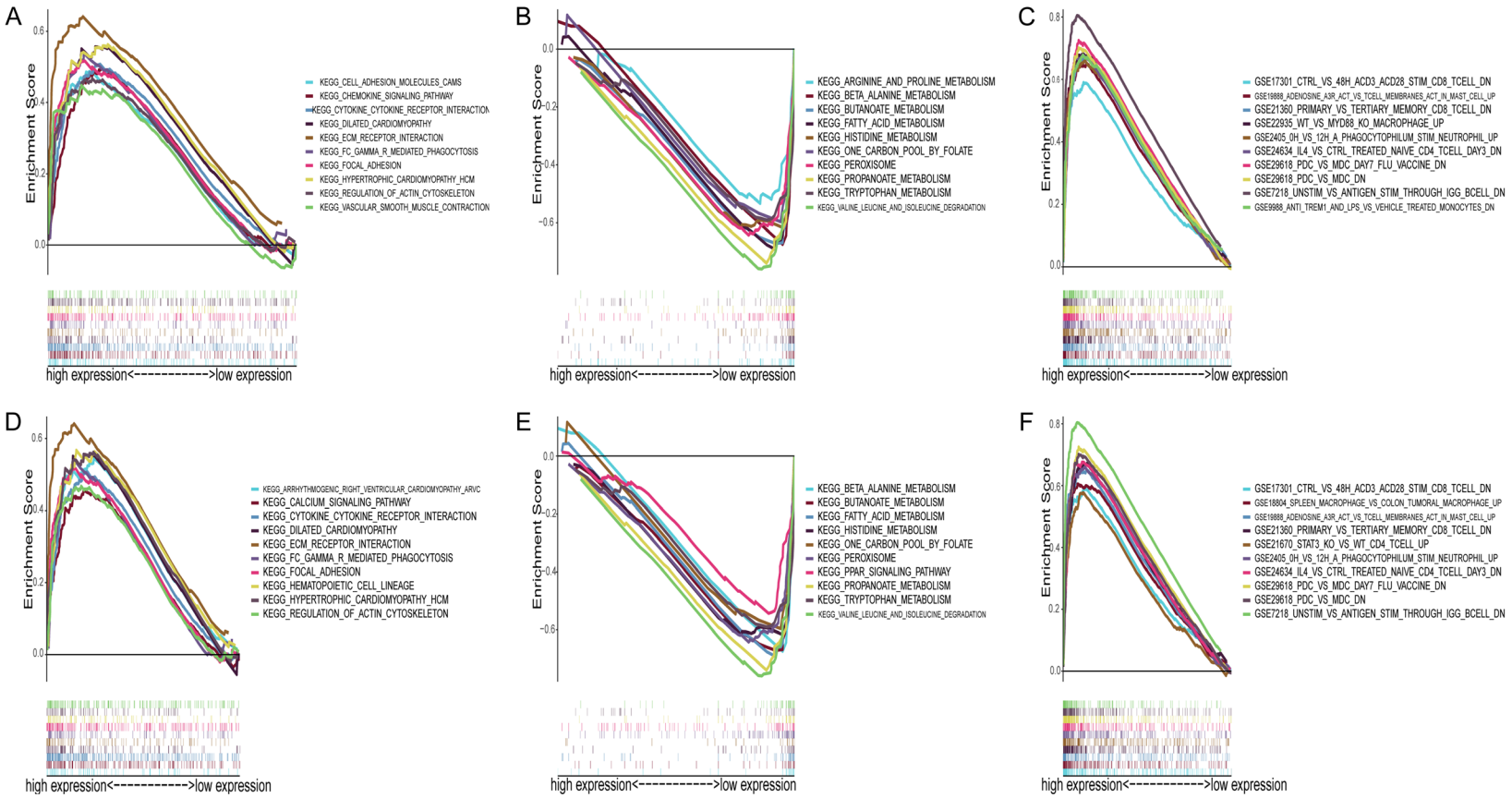

Figure 9. GSEA of TNFSF13B and PPARGC1A. Multi-GSEA enrichment curves for the C2 KEGG collection for (A, D) high TNFSF13B and PPARGC1A expression and (B, E) low TNFSF13B and PPARGC1A expression. (C, F) Multi-GSEA enrichment curves for the C7 collection for high TNFSF13B and PPARGC1A expression.

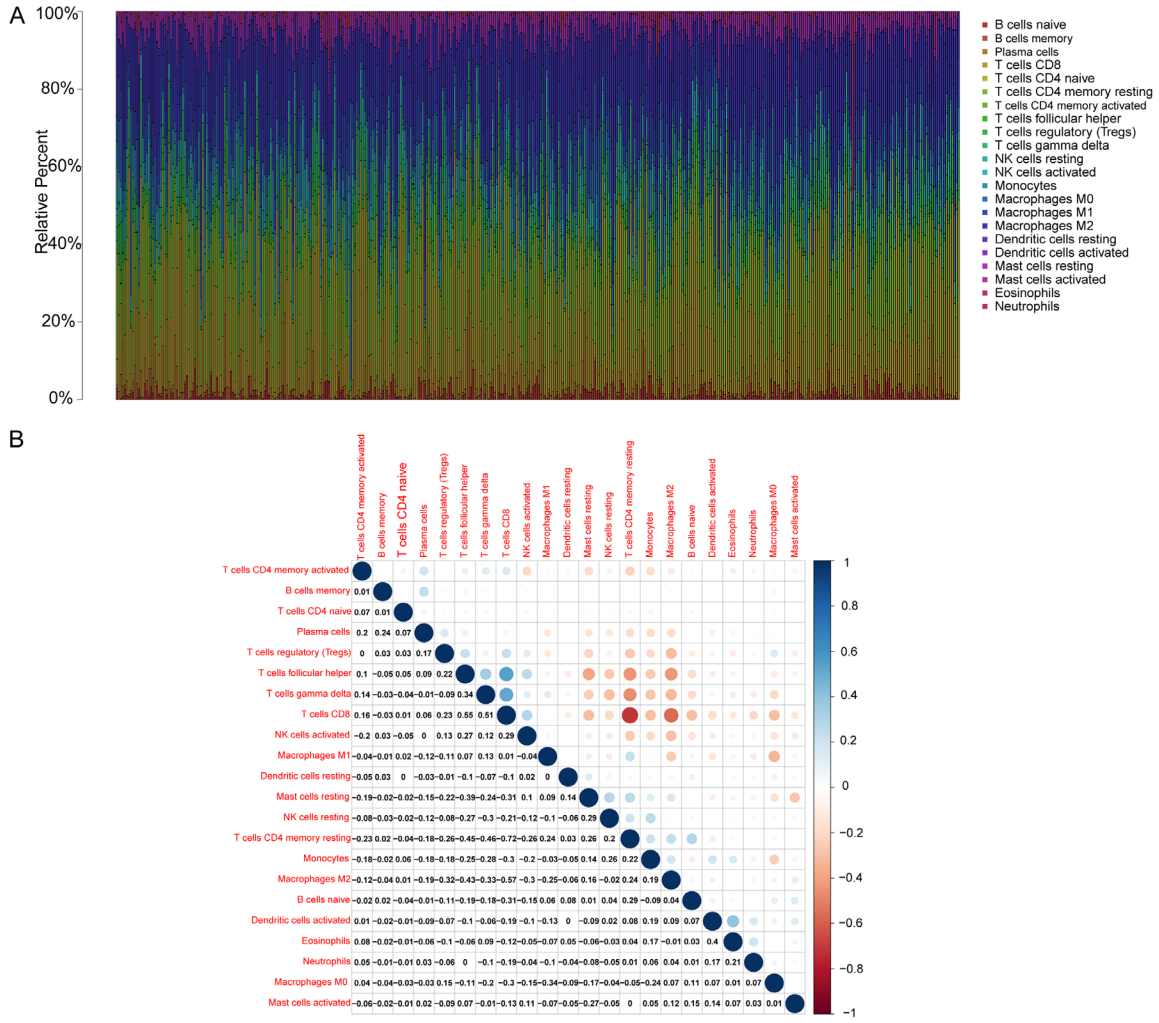

Figure 10. Distribution of TICs in ccRCC tumor samples. A. Proportions of 22 types of TICs in ccRCC samples. B. The heatmap displays the correlation among 22 types of TICs.

TNFSF13B is regulated through a post-transcriptional mechanism [23]. It is worth examining the effect of *TNFSF13B* on TICs further.

PPARGC1A, also known as *PGC-1α*, encodes peroxisome proliferator-activated receptor gamma coactivator-1, a key transcriptional coactivator that coordinates mitochondrial biogenesis and oxidative phosphorylation in tumor cells to induce metastasis [29]. Decreased *PPARGC1A* expression has been related to acute or chronic kidney injury and diabetes [30]. The oncological significance of PPARGC1A expression in tumors remain controversial. Upregulated *PPARGC1A* expression has been shown to promote metastasis in patients with lung cancer [31]. Similar results have been reported in patients with invasive breast cancer [29]. Consistent with our findings, in ccRCC, *PPARGC1A* expression reportedly was significantly lower in tumor tissues than in normal tissues. High *PPARGC1A* mRNA levels were associated with good OS [32]. We observed negative correlations between *PPARGC1A* expression and tumor grade, clinical stage, and M stage in patients with ccRCC. To examine the reasons for these conflicting findings, we used GSEA to identify the affected pathways. In the *PPARGC1A* high expression group, immune-related signaling and epithelial-mesenchymal transition pathways were the most enriched. In the *PPARGC1A* low expression, metabolic pathways, including PPAR signaling and leucine and isoleucine degradation, were highly enriched. All these pathways are associated with oncogenesis. Based on these findings, we

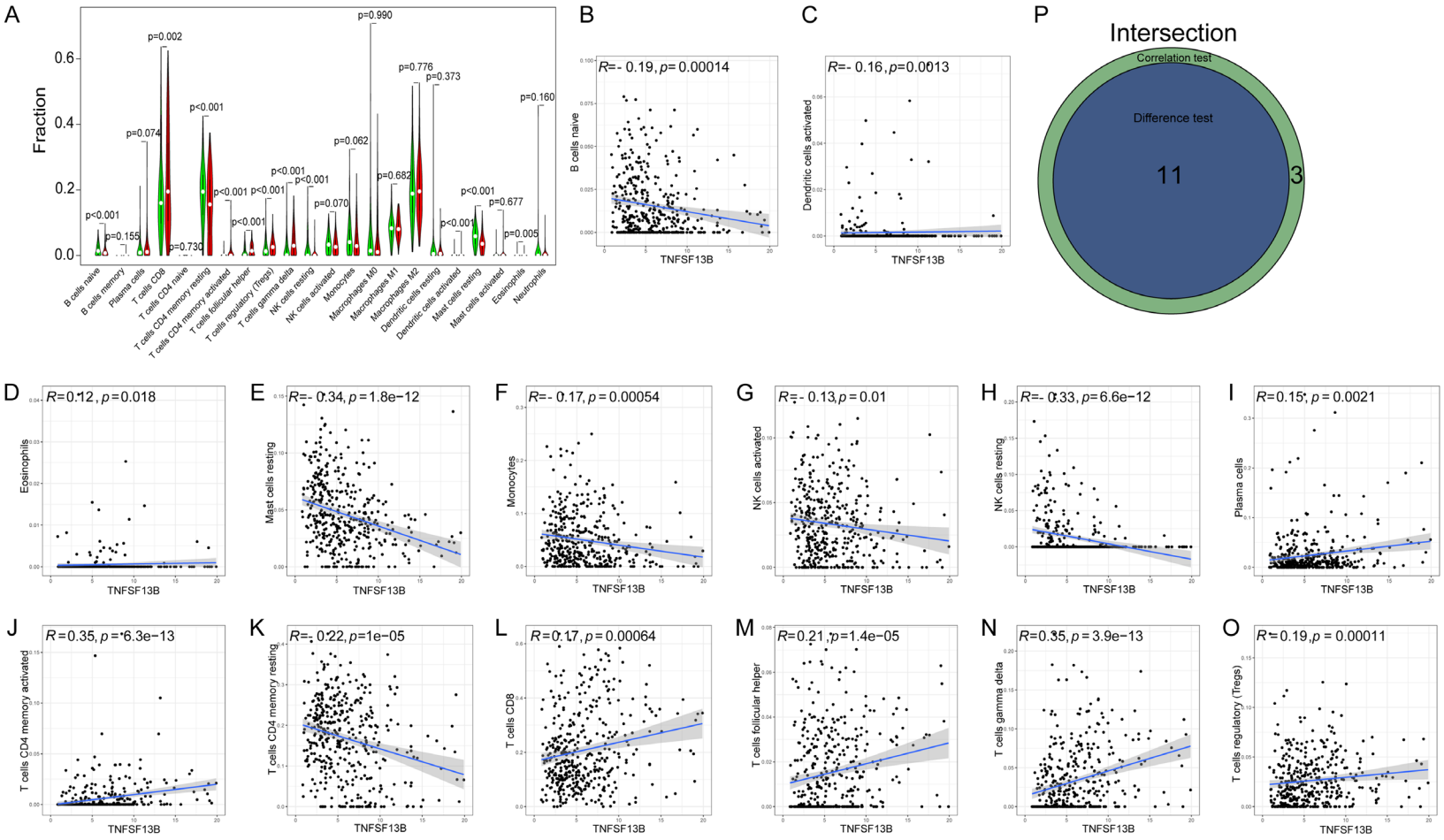

Figure 11. Correlations between TNFSF13B expression and TICs. A. Proportions of 22 TIC types in ccRCC samples with differential expression of TNFSF13B. B-O. Associations between the proportions of 14 TIC types and TNFSF13B expression. P. Venn diagram illustrating 11 types of common TICs correlated with TNFSF13B expression codetermined by difference and correlation tests.

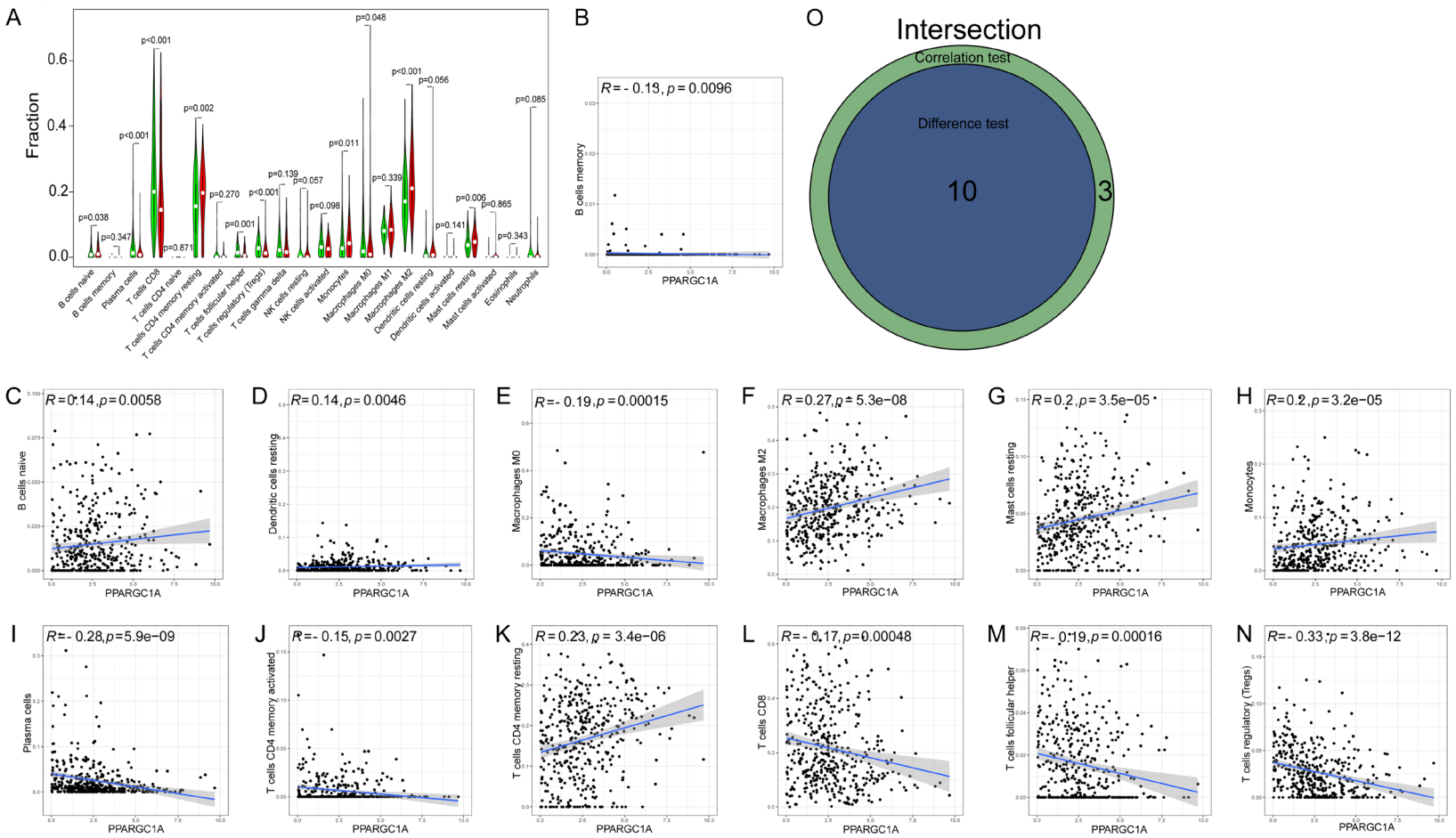

Figure 12. Correlation between PPARGC1A expression and TICs. A. Proportions of 22 TIC types in ccRCC samples with differential PPARGC1A expression. B-N. Associations between the proportions of 13 TIC types and PPARGC1A expression. O. Venn diagram illustrating 10 common types of TICs correlated with PPARGC1A expression codetermined by difference and correlation tests.

speculate that *PPARGC1A* is involved in shifting the TME from immune-dominant to metabolic-dominant and therefore, *PPARGC1A* downregulation is associated with the dismal outcomes of ccRCC.

Considering the crucial roles of *TNFSF13B* and *PPARGC1A* in the immune response in ccRCC, we assessed immune cell infiltration in ccRCC tumor tissues and screened the TICs associated with *TNFSF13B* and *PPARGC1A* using CIBERSORT analysis. We found that *TNFSF13B* expression was positively correlated with the abundances of activated CD4 memory T cells, Tregs, and CD8 T cells. *PPARGC1A* expression was negatively correlated with abundances of Tregs and CD8 T-cells. CD4 T-cells infiltration facilitates RCC cell proliferation by mediating the TGF-β1/YBX1/HIF2α signaling pathway [33]. CD8 T cells infiltration is associated with good prognosis in most cancers, including bladder and lung cancers [34]. The role of CD8 T cells in cancer prognosis and treatment remains unclear. Consistent with our findings, Xiong et al. reported that infiltrating CD8 T cells were associated with worse RCC prognosis [10]. The authors suggested that immunosuppressive immune cells, such as Tregs, may inhibit the antitumor role of CD8 T cells [10]. The activation/inhibition status of CD8 T cells may affect the efficacy of immunotherapies in RCC [35]. Tregs, a type of CD4 T cells with immunosuppressive effects, can promote tumor development and progression by suppressing antitumor immunity [36]. An early study on RCC revealed that Tregs abundance was negatively associated with outcome [37]. Tregs express numerous immune checkpoint molecules. Treg-targeted therapies have become a research focal point [38, 39]. Basic and translational research is required to establish and validate the clinical effects of such treatments. Our TIC analysis suggested that *TNFSF13B* and *PPARGC1A* may participate in the balancing and modulation of immune activity in the TME in ccRCC.

This study had several limitations. The retrospective design of our study allowed for the existence of confounding factors. The scope was limited, so we did not examine how the other three TME-related genes (*IGLL5*, *MZB1*, and *HSD11B1*) are associated with TICs. We did not identify the mechanisms by which all these TME-related prognostic genes participate in ccRCC.

Conclusion

In conclusion, we identified five TME-related genes with prognostic value in ccRCC using the ESTIMATE algorithm. *TNFSF13B* and *PPARGC1A* were significantly associated with changes in the TME. Their roles as indicators of treatment efficacy and potential therapeutic targets should be further examined.

Acknowledgements

This study was supported by the National Key Research and Development Program of China (grant number: 2018YFC2002202). We would like to thank Editage (www.editage.cn) for English language editing.

Disclosure of conflict of interest

None.

Address correspondence to: Dr. Yaoguang Zhang, Department of Urology, Beijing Hospital, National Center of Gerontology, Institute of Geriatric Medicine, Chinese Academy of Medical Sciences, 1 DaHua Road, Dong Dan, Beijing 100730, China. Tel: +86-010-85136272; Fax: +86-010-65132969; E-mail: zhang003887@sina.com

References

[1] Bray F, Ferlay J, Soerjomataram I, Siegel RL, Torre LA and Jemal A. Global cancer statistics 2018: GLOBOCAN estimates of incidence and mortality worldwide for 36 cancers in 185 countries. CA Cancer J Clin 2018; 68: 394-424.

[2] Siegel RL, Miller KD and Jemal A. Cancer statistics, 2020. CA Cancer J Clin 2020; 70: 7-30.

[3] Ljungberg B, Albiges L, Abu-Ghanem Y, Bensalah, K, Dabestani S, Fernández-Pello S, Giles RH, Hofmann F, Hora M, Kuczyk MA, Kuusk T, Lam TB, Marconi L, Merseburger AS, Powles T, Staehler M, Tahbaz R, Volpe A and Bex A. European association of urology guidelines on renal cell carcinoma: the 2019 update. Eur Urol 2019; 75: 799-810.

[4] Maacha S, Bhat AA, Jimenez L, Raza A, Haris M, Uddin S and Grivel JC. Extracellular vesicles-mediated intercellular communication: roles in the tumor microenvironment and anticancer drug resistance. Mol Cancer 2019; 18: 55.

[5] Lan H, Zhang W, Jin K, Liu Y and Wang Z. Modulating barriers of tumor microenvironment through nanocarrier systems for improved cancer immunotherapy: a review of current status and future perspective. Drug Deliv 2020; 27: 1248-1262.

[6] Hinshaw DC and Shevde LA. The tumor microenvironment innately modulates cancer progression. Cancer Res 2019; 79: 4557-4566.

[7] Albini A, Bruno A, Noonan DM and Mortara L. Contribution to tumor angiogenesis from innate immune cells within the tumor microenvironment: implications for immunotherapy. Front Immunol 2018; 9: 527.

[8] Mantovani A, Ponzetta A, Inforzato A and Jaillon S. Innate immunity, inflammation and tumour progression: double-edged swords. J Intern Med 2019; 285: 524-532.

[9] Qi Y, Xia Y, Lin Z, Qu Y, Qi Y, Chen Y, Zhou Q, Zeng H, Wang J, Chang Y, Bai Q, Wang Y, Zhu Y, Xu L, Chen L, Kong Y, Zhang W, Dai B, Liu L, Guo J and Xu J. Tumor-infiltrating $CD39^{+}CD8^{+}$ T cells determine poor prognosis and immune evasion in clear cell renal cell carcinoma patients. Cancer Immunol Immunother 2020; 69: 1565-1576.

[10] Xiong Y, Wang Z, Zhou Q, Zeng H, Zhang H, Liu Z, Huang Q, Wang J, Chang Y, Xia Y, Wang Y, Liu L, Zhu Y, Xu L, Dai B, Bai Q, Guo J and Xu J. Identification and validation of dichotomous immune subtypes based on intratumoral immune cells infiltration in clear cell renal cell carcinoma patients. J Immunother Cancer 2020; 8: e000447.

[11] Bi KW, Wei XG, Qin XX and Li B. BTK has potential to be a prognostic factor for lung adenocarcinoma and an indicator for tumor microenvironment remodeling: a study based on TCGA data mining. Front Oncol 2020; 10: 424.

[12] Jiang M, Lin J, Xing H, An J, Yang J, Wang B, Yu M and Zhu Y. Microenvironment-related gene $TNFSF_{13}B$ predicts poor prognosis in kidney renal clear cell carcinoma. PeerJ 2020; 8: e9453.

[13] Cao J, Yang X, Li J, Wu H, Li P, Yao Z, Dong Z and Tian J. Screening and identifying immune-related cells and genes in the tumor microenvironment of bladder urothelial carcinoma: Based on TCGA database and bioinformatics. Front Oncol 2020; 9: 1533.

[14] Xie L, Wang Q, Dang Y, Ge L, Sun X, Li N, Han Y, Yan Z, Zhang L, Li Y, Zhang H and Guo X. OSkirc: a web tool for identifying prognostic biomarkers in kidney renal clear cell carcinoma. Future Oncol 2019; 15: 3103-3110.

[15] Gupta K, Miller JD, Li JZ, Russel MW and Charbonneau C. Epidemiologic and socioeconomic burden of metastatic renal cell carcinoma (mRCC): a literature review. Cancer Treat Rev 2008; 34: 193-205.

[16] Choueiri TK and Motzer RJ. Systemic therapy for metastatic renal-cell carcinoma. N Engl J Med 2017; 376: 354-366.

[17] Rini BI and Atkins MB. Resistance to targeted therapy in renal-cell carcinoma. Lancet Oncol 2009; 10: 992-1000.

[18] Hakimi AA, Voss MH, Kuo F, Sanchez A, Liu M, Nixon BG, Vuong L, Ostrovnaya I, Chen YB, Reuter V, Riaz N, Cheng Y, Patel P, Marker M, Reising A, Li MO, Chan TA and Motzer RJ. Transcriptomic profiling of the tumor microenvironment reveals distinct subgroups of clear cell renal cell cancer: data from a randomized phase III trial. Cancer Discov 2019; 9: 510-525.

[19] Escudier B, Porta C, Schmidinger M, Rioux-Leclercq N, Bex A, Khoo V, Gruenvald V and Horwich A; ESMO Guidelines Committee. Electronic address: clinicalguidelines@esmo.org. Renal cell carcinoma: ESMO clinical practice guidelines for diagnosis, treatment and follow-up. Ann Oncol 2019; 30: 706-720.

[20] Mori K, Mostafaei H, Miura N, Karakiewicz PI, Luzzago S, Schmidinger M, Bruchbacher A, Pradere B, Egawa S and Shariat SF. Systemic therapy for metastatic renal cell carcinoma in the first-line setting: a systematic review and network meta-analysis. Cancer Immunol Immunother 2021: 70: 265-273.

[21] Simonaggio A, Epaillard N, Pobel C, Moreira M, Oudard S and Vano YA. Tumor microenvironment features as predictive biomarkers of response to immune checkpoint inhibitors (ICI) in metastatic clear cell renal cell carcinoma (mccRCC). Cancers (Basel) 2021; 13: 231.

[22] Chen M, Lin X, Liu Y, Li Q, Deng Y, Liu Z, Brand F, Guo Z, He X, Ryffel B and Zheng SG. The function of BAFF on T helper cells in autoimmunity. Cytokine Growth Factor Rev 2014; 25: 301-305.

[23] Stelmach P, Pütz M, Pollmann R, Happel M, Stei S, Schlegel K, Seipelt M, Eienbröker C, Eming R, Mandic R, Huber M and Tackenberg B. Alternative splicing of the TNFSF13B (BAFF) pre-mRNA and expression of the BAFFX1 isoform in human immune cells. Gene 2020; 760: 145021.

[24] Steri M, Orrù V, Idda ML, Pitzalis M, Pala M, Zara I, Sidore C, Faà V, Floris M, Deiana M, Asunis I, Porcu E, Mulas A, Piras MG, Lobina M, Lai S, Marongiu M, Serra V, Marongiu M, Sole G, Busonero F, Maschio A, Cusano R, Cuccuru G, Deidda F, Poddie F, Farina G, Dei M, Virdis F, Olla S, Satta MA, Pani M, Delitala A, Cocco E, Frau J, Coghe G, Lorefice L, Fenu G, Ferrigno P, Ban M, Barizzone N, Leone M, Guerini FR, Piga M, Firinu D, Kockum I, Lima Bomfim I, Olsson T, Alfredsson L, Suarez A, Carreira PE, Castillo-Palma MJ, Marcus JH, Congia M, Angius A, Melis M, Gonzalez A, Alarcón Riquelme ME, da Silva BM, Marchini M, Danieli MG, Del Giacco

S, Mathieu A, Pani A, Montgomery SB, Rosati G, Hillert J, Sawcer S, D'Alfonso S, Todd JA, Novembre J, Abecasis GR, Whalen MB, Marrosu MG, Meloni A, Sanna S, Gorospe M, Schlessinger D, Fiorillo E, Zoledziewska M and Cucca F. Overexpression of the cytokine BAFF and autoimmunity risk. N Engl J Med 2017; 376: 1615-1626.

[25] González-Serna D, Ortiz-Fernández L, Vargas S, García A, Raya E, Fernández-Gutierrez B, López-Longo FJ, Balsa A, González-Álvaro I, Narvaez J, Gómez-Vaquero C, Sabio JM, García-Portales R, González-Escribano MF, Tolosa C, Carreira P, Kiemeney L, Coenen MJH, Witte T, Schneider M, González-Gay MA and Martín J. Association of a rare variant of the *TNFSF13B* gene with susceptibility to rheumatoid arthritis and systemic lupus erythematosus. Sci Rep 2018; 8: 8195.

[26] Pelekanou V, Notas G, Kampa M, Tsentelierou E, Stathopoulos EN, Tsapis A and Castanas E. BAFF, APRIL, TWEAK, BCMA, TACI and Fn14 proteins are related to human glioma tumor grade: immunohistochemistry and public microarray data meta-analysis. PLoS One 2013; 8: e83250.

[27] Kampa M, Notas G, Stathopoulos EN, Tsapis A and Castanas E. The TNFSF members APRIL and BAFF and their receptors TACI, BCMA, and BAFFR in oncology, with a special focus in breast cancer. Front Oncol 2020; 10: 827.

[28] Luo J, Xie Y, Zheng Y, Wang C, Qi F, Hu J and Xu Y. Comprehensive insights on pivotal prognostic signature involved in clear cell renal cell carcinoma microenvironment using the ESTIMATE algorithm. Cancer Med 2020; 9: 4310-4323.

[29] LeBleu VS, O'Connell JT, Gonzalez Herrera KN, Wikman H, Pantel K, Haigis MC, Machado de Carvalho F, Damascena A, Domingos Chinen LM, Rocha RM, Asara JM and Kalluri R. PGC-1α mediates mitochondrial biogenesis and oxidative phosphorylation in cancer cells to promote metastasis. Nat Cell Biol 2014; 16: 992-15, 1-15.

[30] Li SY and Susztak K. The role of peroxisome proliferator-activated receptor γ coactivator 1α (PGC-1α) in kidney disease. Semin Nephrol 2018; 38: 121-126.

[31] Li JD, Feng QC, Qi Y, Cui G and Zhao S. PPARGC1A is upregulated and facilitates lung cancer metastasis. Exp Cell Res 2017; 359: 356-360.

[32] Xu WH, Xu Y, Wang J, Wan FN, Wang HK, Cao DL, Shi GH, Qu YY, Zhang HL and Ye DW. Prognostic value and immune infiltration of novel signatures in clear cell renal cell carcinoma microenvironment. Aging (Albany NY) 2019; 11: 6999-7020.

[33] Wang Y, Wang Y, Xu L, Lu X, Fu D, Su J, Geng H, Qin G, Chen R, Quan C, Niu Y and Yue D. CD4+ T cells promote renal cell carcinoma proliferation via modulating YBX1. Exp Cell Res 2018; 363: 95-101.

[34] Fridman WH, Zitvogel L, Sautès-Fridman C and Kroemer G. The immune contexture in cancer prognosis and treatment. Nat Rev Clin Oncol 2017; 14: 717-734.

[35] Giraldo NA, Becht E, Vano Y, Petitprez F, Lacroix L, Validire P, Sanchez-Salas R, Ingels A, Oudard S, Moatti A, Buttard B, Bourass S, Germain C, Cathelineau X, Fridman WH and Sautès-Fridman C. Tumor-infiltrating and peripheral blood T-cell immunophenotypes predict early relapse in localized clear cell renal cell carcinoma. Clin Cancer Res 2017; 23: 4416-4428.

[36] Togashi Y, Shitara K and Nishikawa H. Regulatory T cells in cancer immunosuppression-implications for anticancer therapy. Nat Rev Clin Oncol 2019; 16: 356-371.

[37] Cancer Genome Atlas Research Network. Comprehensive molecular characterization of clear cell renal cell carcinoma. Nature 2013; 499: 43-49.

[38] Rini BI, Powles T, Atkins MB, Escudier B, McDermott DF, Suarez C, Bracarda S, Stadler WM, Donskov F, Lee JL, Hawkins R, Ravaud A, Alekseev B, Staehler M, Uemura M, De Giorgi U, Mellado B, Porta C, Melichar B, Gurney H, Bedke J, Choueiri TK, Parnis F, Khaznadar T, Thobhani A, Li S, Piault-Louis E, Frantz G, Huseni M, Schiff C, Green MC and Motzer RJ; IMmotion151 Study Group. Atezolizumab plus bevacizumab versus sunitinib in patients with previously untreated metastatic renal cell carcinoma (IMmotion151): a multicentre, open-label, phase 3, randomised controlled trial. Lancet 2019; 393: 2404-2415.

[39] Huijts CM, Lougheed SM, Bodalal Z, van Herpen CM, Hamberg P, Tascilar M, Haanen JB, Verheul HM, de Gruijl TD and van der Vliet HJ; Dutch WIN-O Consortium. The effect of everolimus and low-dose cyclophosphamide on immune cell subsets in patients with metastatic renal cell carcinoma: results from a phase I clinical trial. Cancer Immunol Immunother 2019; 68: 503-515.